AJNR

Functional applications of CT of the central nervous system.

B P Drayer

AJNR Am J Neuroradiol 1981, 2 (6) 495-510
http://www.ajnr.org/content/2/6/495

Special Article

Functional Applications of CT of the Central Nervous System

Burton P. Drayer[1]

Although CT has developed as a morphologic technique, its anatomic specificity may be used to map physiologic events. Using intravenously infused iodinated contrast media, CT offers unique analysis of the integrity of the blood-brain barrier. If the barrier is not disrupted, the same iodinated indicators may be used to estimate vascular transit time and cerebral blood volume. Nonradioactive xenon, a freely diffusible indicator, enhances the brain substance and may be used to evaluate both cerebral blood flow and tissue integrity in well defined anatomic locales. However, these functional determinations have distinct limitations. Future use of CT, including providing more sophisticated tissue characterization, indicator development, and advances in scanner technology, are discussed.

Transmission computed tomography (CT) was initially developed as a noninvasive morphologic technique from which functional information could sometimes be indirectly surmised. However, the contrast sensitivity, spatial resolution, and temporal resolution provided by present scanners makes CT a unique imaging method for characterizing, in vivo, physiologic or metabolic events with anatomic specificity.

Although recent interest in these applications has been keen, we must remain cognizant of various pitfalls when drawing physiologic conclusions from CT-derived information. Some key problems involve the quantitative accuracy of the derived CT numbers, the need for multilevel scanning, signal to radiation dose compromises, and the requirement for contrast media that truly reflect metabolic events while providing sufficient enhancement at nontoxic doses.

This review attempts to summarize the developments that have occurred over the past few years in functional CT imaging of the brain. The present limitations of these new techniques are brought out and suggestions are offered that would enhance the application of CT to functional assessment of the central nervous system.

Applications of Dynamic CT

Blood-Brain Barrier

The initial and most widely used physiologic application of CT scanning involves an analysis of alterations in the blood-brain barrier. The normal barrier is essentially impermeable to intravenously infused iodinated contrast media. With certain pathologic processes (e.g., neoplasm, abscess, infarctions), the barrier is damaged causing leakage of iodine with resultant abnormal "contrast enhancement" on CT.

The normal blood-brain barrier. Current concepts concerning the barrier [1–4] suggest that it consists of nonfenestrated capillary endothelial cells with tight junctions (zona occludens) interposed and an overlying basement membrane

Received June 6, 1981; accepted after revision July 14, 1981.

This work was supported by a grant-in-aid from the American Heart Association with funds contributed by the North Carolina Heart Association.

[1]Department of Radiology, Duke University Medical Center, Durham, NC 27710.

***AJNR* 2:495–510, November/December 1981**
0195-6108/81/0206-0495 $00.00

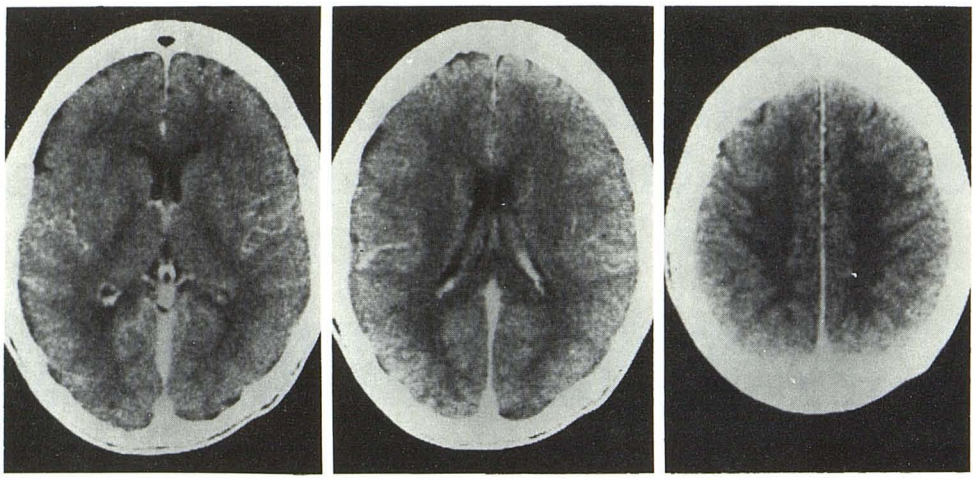

Fig. 1.—Normal brain with iodinated contrast medium (nondiffusible indicator). Prominent enhancement in gray matter capillary bed highlights distinction between gray and white matter. Gray matter has about four times the capillary density and perfusion as white matter.

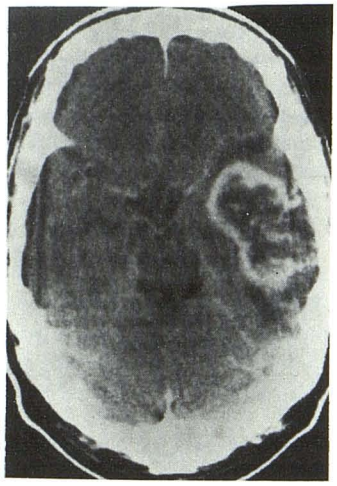

Fig. 2.—Breakdown of blood-brain barrier. Glioblastoma multiforme of temporal lobe with prominent contrast enhancement.

separating the endothelial cells and tight junctions from the extracellular brain space and glial foot processes. Movement across the normal barrier occurs by either lipid-mediated transport of lipid-soluble compounds or carrier-mediated transport of water-soluble substances [5]. Specific regions of the brain, the circumventricular organs (area postrema, median eminence of the hypothalamus, organ vasculosum of the lamina terminalis, subfornical organ, pineal, and the lines of attachment of the choroid plexus), possess no such endothelial barrier and presumably provide information to the brain concerning the chemical environment of the rest of the body.

Substances cross the barrier with variable ease dependent predominantly on lipid solubility, but also on polarity, molecular size, and enzymatic degradation. Water and gases (CO_2, O_2, Xe, Kr, volatile anesthetics) rapidly diffuse across the intact barrier. Since diffusion across the barrier is directly correlated to lipid solubility, highly lipid-soluble substances (ethanol, iodoantipyrine, thiopental) readily pass the barrier. The passage of nonionized lipophilic substances (e.g., NH_2) is pH dependent. Simple charged ions (e.g., Na+, K+), neutral, basic, and acidic amino acids, monocarboxylic acids, amines, purines, nucleosides, and hexoses (deoxyglucose, d-glucose but not l-glucose) cross the barrier by carrier-mediated transport [5]. Enzymatic degradation in the capillary endothelium may retard the transport of neurotransmitter precursors [1, 6–8]. In contrast to peripheral capillaries, pinocytosis normally plays only a minor role in transport but may be important in the diseased barrier [8].

Experimentally, the integrity of the barrier may be illustrated by confirming that a nondiffusible indicator (e.g., Evans blue dye, horseradish peroxidase) [2], injected intravenously, does not cross the barrier into the brain. This same principle, when applied in vivo, forms the basis for radionuclide brain scanning using nondiffusible technetium or gallium derivatives and CT scanning using the nondiffusible iodinated contrast media.

If the barrier is intact, a focal accumulation of nondiffusible indicator will not be found in the brain substance, although contrast enhancement may be apparent in brain regions not protected by the barrier. Increased density on CT is often prominent in the large intracranial vascular channels and the capillary bed of the gray matter (fig. 1) in the initial period after indicator infusion [9–13]. On a delayed scan at 45 min after infusion, the intracranial density has returned to baseline.

The pathologic blood-brain barrier. A fundamental principle of clinical radiodiagnostic methodology over the past two decades has involved analysis of the integrity of the barrier using intravenously infused radionuclides or iodinated contrast media. The introduction of an iodinated vascular tracer has become almost routine in cranial CT. Various pathologic processes including neoplasm, abscess, infarction, and acute demyelination may alter the barrier (fig. 2), permitting leakage of contrast material into the extravascular brain space [14–16]. A disrupted barrier may also result from acute severe hypertension, seizures, hy-

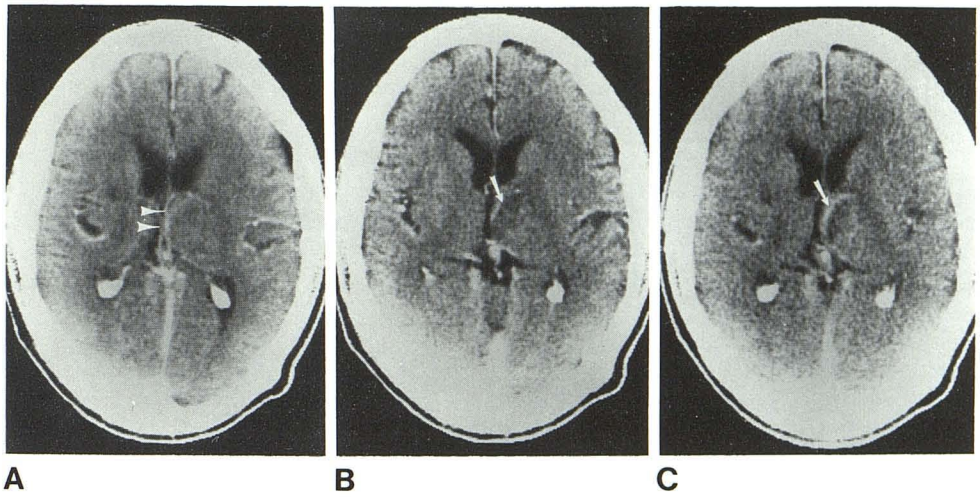

Fig. 3.—Breakdown of blood-brain barrier, cerebral infarction (day 7). **A**, CT immediately after intravenous infusion of 42 g of iodinated contrast medium. Subtle stretching and displacement of internal cerebral veins (*arrowheads*). **B**, 25 min delayed CT. Minimal enhancement (*arrow*) intermixed with decreased density in region of thalamus and posterior limb of internal capsule. Mild shift of posterior III ventricle. **C**, 50 min delayed CT. Far more definitive representation of abnormal enhancement (*arrow*) in thalamus due to accumulation of contrast medium that has crossed excessively permeable blood-brain barrier. Visualization of posterior limb of internal capsule may reflect associated edema.

percapnia, acidosis, concussion, markedly elevated intracranial pressure, and even the intracarotid infusion of concentrated iodinated contrast media [4, 17–20]. Various theories have been proposed to explain the barrier breakdown including stimulation of pinocytosis, opening of tight junctions, and endothelial proliferation. In fact, the mechanism may differ depending on the disease process.

In most individuals, the intravenous infusion of 42 g of iodine in a 150 or 300 ml volume is sufficient to detect a barrier abnormality using CT imaging. Some have suggested that larger doses of contrast media will improve diagnostic accuracy [21–23], but controversy exists concerning the increased potential for adverse reactions (renal [24] and/or cerebral toxicity). Most agree that by obtaining a delayed CT scan at 30–90 min after the infusion of contrast material, additional information concerning the presence and extent of blood-brain barrier damage becomes available (fig. 3). Although clinical history, patient age, anatomic locale, and associated edema pattern [25, 26] may assist the clinician in making an accurate "educated guess" concerning the ultimate pathologic diagnosis, the actual pattern and degree of breakdown have not yet proven consistently disease specific.

The contrast-enhancement ratio (CER) seems the most direct measure of barrier integrity of disruption, and early CT studies did not define any ratio that was specific for a pathologic process [14, 15].

$$CER = \frac{\Delta\ CT\ \#\ Brain\ (Enhanced,\ time\ T - Baseline)}{\Delta\ CT\ \#\ Blood\ (Enhanced,\ time\ T - Baseline)}$$

Dual kilovoltage techniques [27–29] (analysis of changes in effective atomic number) have been used in an attempt to distinguish various tumor types, but the overlap among the different groups makes the use of this strategy tenuous at present, particularly when making the vital and potentially devastating diagnostic and therapeutic decisions that are necessary when treating cerebral neoplasms.

Reversible opening of the blood-brain barrier. By infusing hyperosmotic mannitol or arabinose into the internal carotid artery, Rapoport and associates [4, 19, 30–32] confirmed that the normal barrier may be transiently disrupted with subsequent return to normal within a few hours. Unfortunately, the degree of barrier opening is variable even when using the same dose and infusion rate of a hyperosmotic material [4, 32]. When ultimate tissue analysis has been performed in vitro, Evans blue, horseradish peroxidase, ^{14}C sucrose [30, 32], and ^{14}C deoxyglucose [33] have been used to quantitate the degree of opening. Similar estimations have been performed in vivo using both radionuclides and iodinated contrast media [34, 35] (fig. 4). Higher contrast-enhancement ratios have signified more extensive disruption of the barrier. The major potential applications of hyperosmotic barrier opening include: (1) facilitating greater passage of contrast medium through a barrier only mildly damaged, thus permitting earlier recognition of disease, (2) allowing entry into the brain of a radiopharmaceutical (e.g., labeled antibody or drug) that will define a specific brain function but would not normally cross an intact blood-brain barrier, and (3) permitting greater access of a chemotherapeutic agent or other drug to an area of diseased brain [36–38]. Before use of this technique in man, further studies should be performed to define the toxicity of hyperosmotic barrier opening and the effects of greater direct access of iodinated contrast media to the brain substance.

Transit Time and Cerebral Blood Volume (fig. 5)

The commonly used iodinated contrast media do not significantly cross an intact blood-brain barrier and are considered nondiffusible indicators. Since the intravenous infusion of these indicators has become routine in head CT, many investigators have attempted to extract physiologic information from the passage of these contrast media through the intracranial vasculature [9–13, 39]. Technologic developments have permitted rapid (<3 sec) sequential scanning with good spatial resolution, thereby allowing an

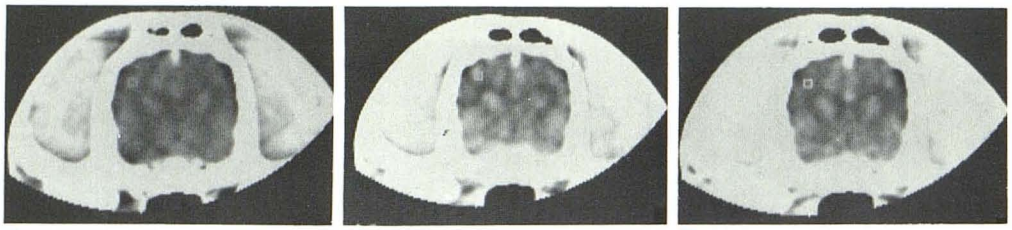

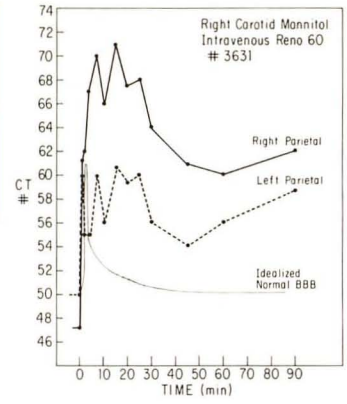

Fig. 4.—Transient opening of blood-brain barrier (BBB), intracarotid mannitol. **A**, Coronal CT scan in dog 5 min after intravenous infusion of 1.25 ml/kg bw of Renografin-60 and 15 min after carotid infusion of 150 ml of 25% mannitol to transiently open BBB. **B**, Same level 20 min after contrast medium infusion. Increasing enhancement bilaterally in deep and cortical gray matter reflecting barrier leakage. Square cursor is in parietal gray matter opposite side of carotid mannitol infusion. **C**, Same level 60 min after intravenous contrast medium (70 min after mannitol). Persistance of brain enhancement. **D**, Graphical representation of contrast enhancement in these scans in left vs. right parietal lobe after BBB disruption with intracarotid mannitol.

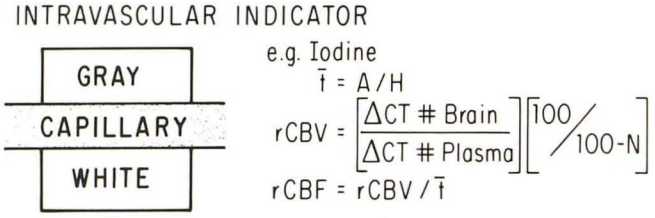

Fig. 5.—Summary of intravascular indicator applications. Currently used intravenously infused iodinated contrast media remain in vascular bed and pass into brain in only negligible amounts if blood-brain barrier is intact. Using dynamic CT, mean transit time ($\bar{t}$) can be estimated from area (A) and height (H) of time-density curve. From static CT image of brain and venous blood in plastic syringe, regional cerebral blood volume (rCBV) can be approximated. Central volume principle as derived by Meier and Zierler states that mean transit time is directly proportional to volume of distribution (rCBV) and inversely proportional to regional blood flow (rCBF).

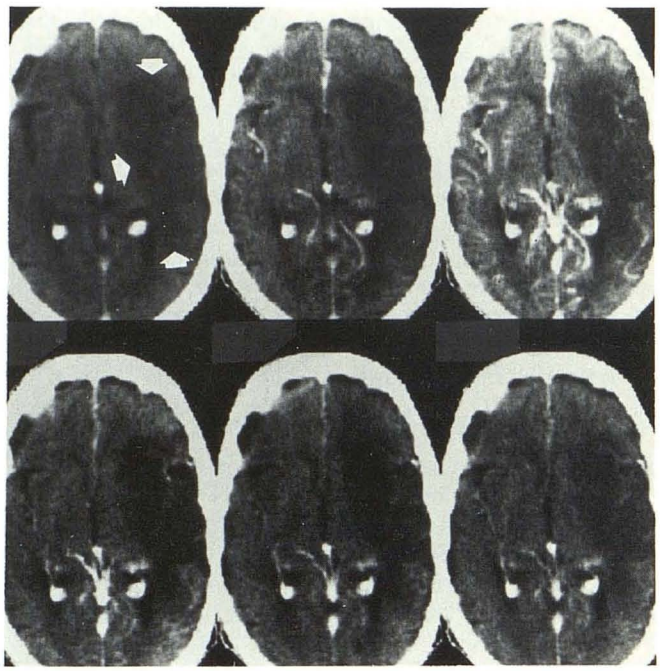

Fig. 6.—Dynamic CT scanning of nondiffusible indicator. After rapid intravenous injection of 49 ml (7 ml/sec for 7 sec) of Renografin-60, serial CT scans were obtained using a 4.8 sec scan time and a 1.0 sec interscan delay in patient with large cerebral infarction (*arrows*) in distribution of middle cerebral artery. Data obtained from these scans were used for mean transit time calculations in figure 7.

analysis of cerebrovascular transit times (fig. 6). Such studies have used principles developed in nuclear medicine imaging while exploiting the more precise anatomic localization provided by CT.

The technique used by most groups for analyzing cerebral transit time involves the rapid (5–10 sec) intravenous (brachial vein) injection of about 50 ml of a high-concentration iodinated contrast medium. Consecutive CT scans at a chosen brain level are then performed every 1–5 sec with the scan sequence begun before contrast material enters the cerebral vasculature so that a baseline (nonenhanced) numerical CT value is available for comparison with the subsequent enhanced scans. Regions of interest in selected brain and vascular locales are then chosen for quantitation by arbitrary visual or defined computerized methods. By plotting the change in CT number (Δ CT #) over a given time interval (time-concentration curve), transit time can be estimated by a variety of methods (fig. 7).

The currently popular strategy for estimating the mean transit time uses the first moment (center of gravity of the shape) of the time-concentration capillary curve obtained from gamma variate curve fitting of the CT derived data [39]. This is based on the theories that the first moment of the draining venous concentration of the contrast medium after a bolus arterial injection most closely represents flow, and that the residual indicator in the intravascular (e.g., brain capillary bed) space as measured by CT will exactly equal (perfect mixing) the concentration in the draining vein. However, mixing is not perfect; this method provides only a relative or approximate transit time which can be useful for comparisons within a given patient but not for calculating actual mean transit time for comparisons among different patients.

It should be remembered that the analysis of indicator dilution curves for calculating mean transit time requires an intracarotid instantaneous bolus injection (delta function) of a small volume of iodinated contrast medium [40–42]. With

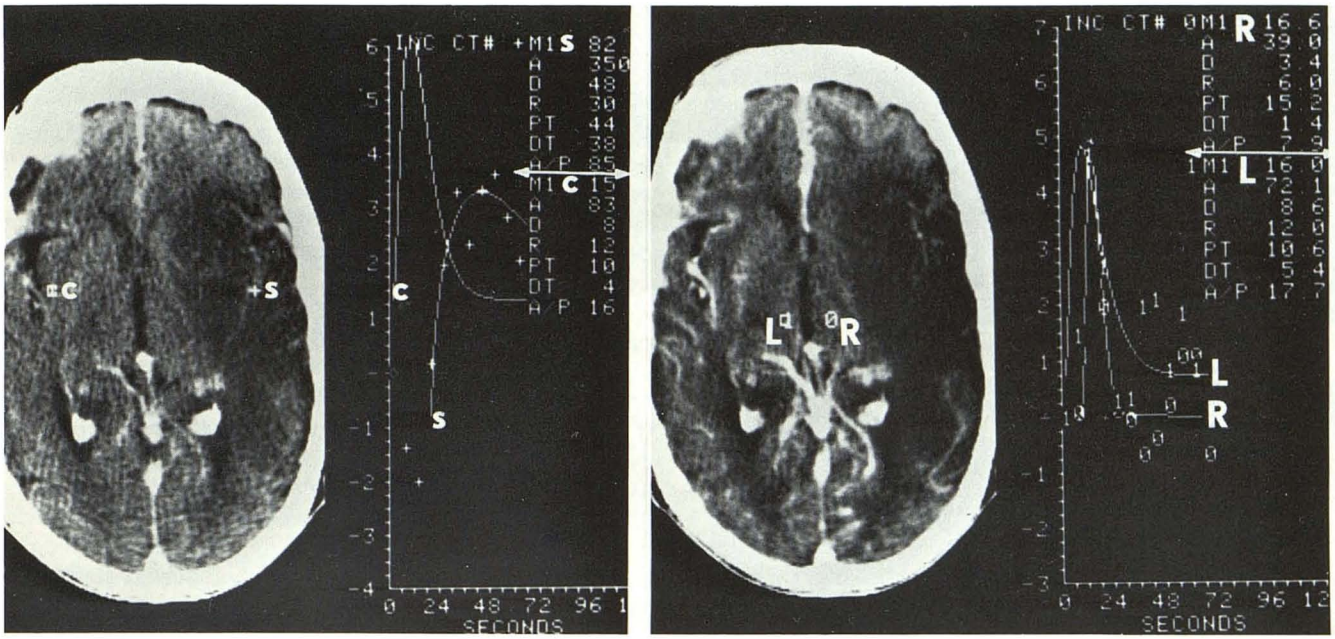

A B

Fig. 7.—Dynamic CT, transit time analysis. **A**, Delayed transit iodinated contrast medium through cerebral infarction(s) in distribution of middle cerebral artery as compared to uninvolved contralateral brain vasculature (c). Mathematical analysis of transit time in this figure was developed at University of California, San Francisco in conjunction with General Electric Corporation. Chosen region of interest (s) exhibited fastest transit time in infarction, while many other regions showed negligible if any increases in CT number. **B**, Transit through thalamic capillary bed (posterior cerebral artery distribution) was symmetric bilaterally (R and L). Transit times were also estimated (not shown here) for occipital regions and were symmetric bilaterally.

a dispersed bolus, such as intravenous infusion of larger quantities of contrast medium, a correction is necessary for the prolonged input. Axel [39] suggested that by directly subtracting the mean injection time from the observed capillary bed transit time, the same mean transit time is obtained as would have been estimated using an instantaneous carotid injection. The mean injection time is determined using a histogram-based region of interest that includes large vessels but excludes gray and white matter capillary beds. Unfortunately, a small region of interest around a major artery on a very thinly collimated scan section would be necessary to avoid significant partial volume averaging when estimating mean injection time. This type of analysis is cumbersome and is limited to small thicknesses of the brain for a given infusion if one wants to calculate an absolute rather than a relative mean transit time.

Another method for circumventing some of the problems created by a dispersed bolus would be to directly infuse (instantaneous bolus) iodinated contrast material into the internal carotid artery at angiography [42–46]. A traditional analysis of the area (A) of the time-concentration residue detection curve divided by the maximum height (H), with a small correction for indicator recirculation, permits the circulation of the mean transit time ($\bar{t}$): $\bar{t} = (A/H)\ min$. This estimation contains error particularly of curve maximum height, as the detecting device (CT scanner) might not initially see the entire bolus when a 5–10 ml volume of iodinated contrast medium is infused over 1–2 sec. More importantly, the obvious advantage of the relatively noninvasive intravenous infusion is lost using the intraarterial method.

It is important to recognize that mean transit time is not a measure of regional cerebral blood flow (rCBF) unless the local blood volume is constant. This has been called the central volume principle and the basic equation as derived by Meier and Zierler [47] states that the mean transit time ($\bar{t}$) is directly proportional to the regional volume of distribution of the indicator (V) and inversely proportional to regional blood flow (F): $\bar{t} = V/F$. When a nondiffusible iodinated contrast medium is used, V is approximately equal to regional cerebral blood volume (rCBV). As variations of more than 100% may exist between the volume (V) of an engorged vs. a collapsed vascular system [42], major difficulties in quantitating rCBF in absolute rather than relative terms using nondiffusible indicators seem apparent.

The estimation of rCBV using CT is relatively straightforward [48, 49]. Intravascularly infused iodinated contrast media are confined to the plasma compartment. rCBV is calculated by dividing the change in the derived CT number from a selected intracranial region of interest by the change in the derived CT number from a simultaneous venous blood sample drawn in a heparinized plastic syringe and placed in a scanning phantom. Using a stimulated x-ray fluorescence technique, Phelps et al. [50] observed that the time lapse between the rapid intravenous infusion of contrast medium and brain/blood scanning is not critical when calculating rCBV.

Certain approximate corrections become necessary when

calculating rCBV. Since iodinated contrast media do not penetrate the red blood cells, a correction is necessary for the ratio of the cerebral to large vessel hematocrit. Most authors use a value of 0.85 derived from average values (range, 0.80–0.92) found in the literature [48, 50, 51]. In addition, after the injection of an iodinated contrast medium, there is a decrease in hematocrit (blood dilution factor, DF) to correct for and a final negligible correction is made for the density (g) of brain tissue (1.04 g/ml). The final operational equation for calculating rCBV is as follows:

$$rCBV = \frac{(CT\,\#\,enhanced - CT\,\#\,baseline)_{Brain} \times 0.85 \times 100}{(CT\,\#\,enhanced - CT\,\#\,baseline)_{Blood} \times DF \times g}\ ml/100\ g$$

The vein of Galen provides a potential substitute for peripheral venous blood; however, partial volume averaging presents a potential error unless thin collimation is used.

Although the rCBV values derived using these CT strategies seem to correlate reasonably well with those obtained using other methods, shortcomings exist that limit consistent quantitation in disease states in man [9, 52, 53]. (1) About 70% of cerebral vascular contrast medium probably resides in venules with only 20% in the capillary bed [43], making perfusion (nutritional flow) assumptions uncertain. This problem is exemplified by the "luxury perfusion" phenomenon [54] where vasoparalysis results in increased arteriovenous perfusion as reflected by regional high density on CT, yet the brain tissue does not receive or benefit from this increased vascular transit (i.e., non-nutritional flow). (2) Significant changes occur in the cerebral circulation after infusion of contrast material [55–58] including alterations in autoregulation, blood pressure, blood volume, and blood flow. (3) A major assumption when using a nondiffusible indicator is that the blood-brain barrier is intact. However, in many pathologic states the barrier is damaged with increased accumulation of contrast medium in the brain while the blood enhancement remains unchanged [9, 53]. (4) The ratio of cerebral to large vessel hematocrit may also be altered with certain pathologic processes and with hyperviscosity. (5) Even large intravenous doses of contrast material produce only limited enhancement in the brain capillary bed. Thus, the error in the derived CT numbers (about ± 1.0 CT units) may be a significant percentage of the ultimate cerebral vasculature enhancement [53]. (6) Patient movement may occur, particularly with rapid intravenous infusion, making comparison of baseline to enhanced regions of interest difficult.

Although the limitations of transit time and blood volume CT determinations must be recognized, relative values may prove clinically useful in understanding the normal brain as well as certain disease processes that do not significantly damage the blood-brain barrier:

Transient ischemic attacks have been studied [13] with the suggestion that four patterns might be shown if the two cerebral hemispheres are compared: (1) normal arterial (arterial transit time) and normal mean capillary transit time (capillary minus arterial transit time); (2) normal arterial with delayed mean capillary transit suggesting impaired tissue perfusion with normal arrival (normal arrival might suggest symmetry or patency of arteries proximal to region of interest vessel); (3) delayed arterial and capillary transit to an equal degree suggesting adequate tissue perfusion but delayed arrival, and (4) delayed arterial to a lesser degree than delayed capillary transit suggesting delayed arrival as well as impaired tissue perfusion.

Cerebral infarctions present a reasonably consistent dynamic CT transit time picture [10–12]. Hypoperfusion is usually reflected by delayed mean transit time and decreased maximum height (Δ CT #) on time-density curve (figs. 6 and 7). Hyperperfusion as indicated during the first pass together with a normal stable distribution image (at 5–10 min after contrast infusion) may be predictive of recovery [12]. It thus seems clinically reasonable to obtain information concerning both transit time (rapid sequence dynamic images) and blood-brain barrier integrity (delayed stable distribution image).

Cerebral edema shows a pattern of normal or delayed transit, reduced maximum CT enhancement, and diminished regional cerebral blood volume (rCBV) [9, 12].

Arteriovenous malformations may have a relatively short transit time with an increased maximum curve height [9, 11].

Cerebral neoplasms have components of increased vascularity and barrier disruption which may be differentiated using the combination of rapid and delayed CT imaging [10–12, 59].

Chronic degenerative diseases (e.g., Alzheimer disease) may be better understood with CT studies of transit time and regional cerebral blood volume, as they do not show evidence of significant barrier damage. Such studies have yet to be performed.

Circulatory arrest as in brain death is suggested by the absence of any large vessel or capillary bed enhancement on either rapid sequence or stable distribution scans after a confirmed successful intravenous infusion of sufficient doses of iodinated contrast material [9, 26, 60, 61].

Therefore, rapid sequence scanning may prove useful in defining relative abnormalities as long as its definite shortcomings are understood and rigid quantitations are not expected. Probably the most useful application of dynamic CT using nondiffusible indicators is not functional but anatomic. The improved and sequential definition of large blood vessels permits the potential distinction of intra- from extraaxial neoplasms [59], better visualization of feeding arteries and draining veins in vascular malformations, and more accurate distinction of an isodense extracerebral hematoma from underlying large vessels and the cortical capillary bed. In addition, when rapid scanning is used in conjunction with rapid table movements, multilevel imaging with multiplane reformatting and three-dimensional reconstruction can be performed to morphologically analyze the carotid bifurcation [62], the supraclinoid carotids, and even the intracranial vasculature (fig. 8). This application, however, may decline in importance with the emergence of digital intravenous angiography [63–66].

Fig. 8.—Normal vascular anatomy using CT and iodinated contrast medium. Coronal reformatting of consecutive 4 mm scans (2 mm scan overlap) performed during continuous intravenous infusion of iodinated contrast medium displays internal carotid, anterior cerebral, and middle cerebral arteries.

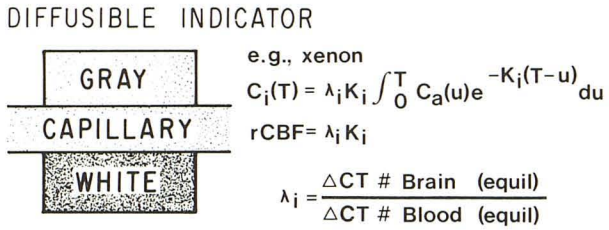

Fig. 9.—Summary of diffusible indicator applications. Diffusible indicator (e.g., xenon) freely crosses intact blood-brain barrier to distribute initially in relation to blood flow (gray > white matter for xenon) and in relation to brain-blood partition coefficient at equilibrium (white > gray matter for xenon). $C_i(T)$ = concentration of xenon in chosen brain locale, ($_i$) at chosen time (T); λ_i = brain-blood partition coefficient; K_i = flow rate constant; C_a = arterial concentration of xenon; rCBF = regional cerebral blood flow.

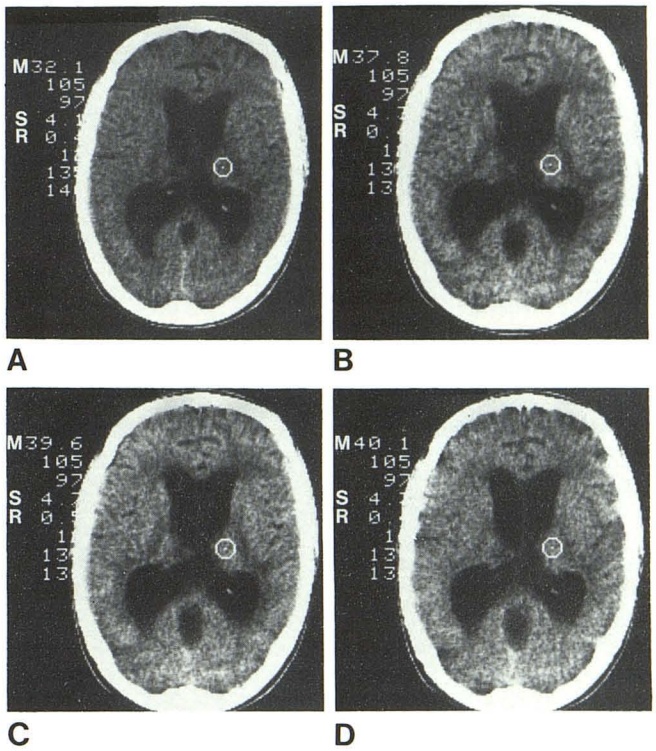

Fig. 10.—Xenon-enhanced CT, buildup analysis of normal thalamus. **A**, Baseline scan just before xenon inhalation; region of interest (ROI) cursor in thalamus. M = mean CT number for chosen ROI; S = standard deviation; and R = root mean square deviation. **B**, Scan at 2 min at same level during xenon (32%) inhalation. Preferential enhancement of gray matter and highlighting of posterior limb of internal capsule (white matter) which enhances less at this early phase of inhalation. CT number has increased 5.7 units (U) (ie., 32.1 to 37.8) in thalamic ROI and would be used for C_i in formula in figure 9. **C**, 6.5 min. Greater enhancement in thalamus (7.5 CT U) and other brain structures as xenon inhalation continues. **D**, 10.5 min. Thalamic gray matter essentially equilibrated with blood at this phase of xenon inhalation. Equilibration confirmed by similar degree of enhancement at 6.5 (7.5 CT U) and 10.5 (8.0 CT U) minutes of inhalation. Posterior limb of internal capsule (white matter) no longer sharply defined, as white matter has not equilibrated and continues to increase in density. If inhalation of xenon were continued for 20–30 min, white matter structures would also equilibrate and become denser (about 15.0 CT U) than gray matter (8.0 CT U).

Cerebral Blood Flow, Diffusible Indicator Methods (fig. 9)

Radionuclide methods for the estimation of regional cerebral blood flow (rCBF) have involved the use of radioactive inert gases, xenon-133 and krypton-85 [42, 54, 67–71]. These techniques have had basic limitations because of poor anatomic specificity and the necessity for using fixed partition coefficients. Emission CT analyses of blood flow are limited at present by high cost, poor spatial resolution, and slow scanning speed [72]. For these reasons, the sequential CT imaging of inhaled nonradioactive xenon [73–78] (figs. 10 and 11) has been developed to provide a high resolution, in vivo, neuroanatomic map of tissue perfusion (nutritional blood flow) [79–83] and brain-blood partitioning [76, 79–82]. Xenon, an inert gas that readily diffuses across the blood-brain barrier, has a k-edge similar to that of iodine, permitting imaging with x-rays. Due to its inertness and diffusibility, useful measurements of brain blood flow and brain-blood partition coefficient have been obtained with this gas.

A brief review of the theoretical concepts underlying this calculation of rCBF is offered to facilitate the understanding of the relatively straightforward data obtained using xenon-enhanced CT scanning. This discussion draws on the reviews of Siesjo [84] and Lassen and Ingvar [42]. A detailed analysis of the mathematical principles has been amply analyzed in previous studies and is beyond the scope of this review.

As stated earlier, the equation of Meier and Zierler ($\bar{t} = V/F$) is the basis for measuring cerebral blood flow [47]. The equation is derived from the principle of conservation of matter and states that indicator particles introduced into a perfused organ must be cleared from it. Kety [67] was the first to understand the superiority of inert gases as diffusible indicators for blood flow measurements. He noted that inert gases dissolve physically in all brain compartments, have similar solubility in brain as in blood, are essentially unaffected by large changes in local cerebral blood volume, and at equilibrium are distributed passively according to solubility properties (partition coefficient).

In his inert gas method, Kety applied the Fick principle to a nonsteady state situation. Since inert gases are not metabolized by the brain, the amount of gas taken up by the brain (Q_i) ($_i$ representing a selected tissue compartment) in a given time interval (T) is the difference between the arterial input (Q_a) and the venous outflow (Q_v): $Q_i(T) = Q_a(T) - Q_v(T)$. If arterial inflow equals venous outflow, for any given instant the equation can be written: $(dC_i/dt) = (F_i/V_i)(C_a - C_v)$, where C_a is the arterial concentration and C_v the venous concentration. Since the arterial input equals the arterial

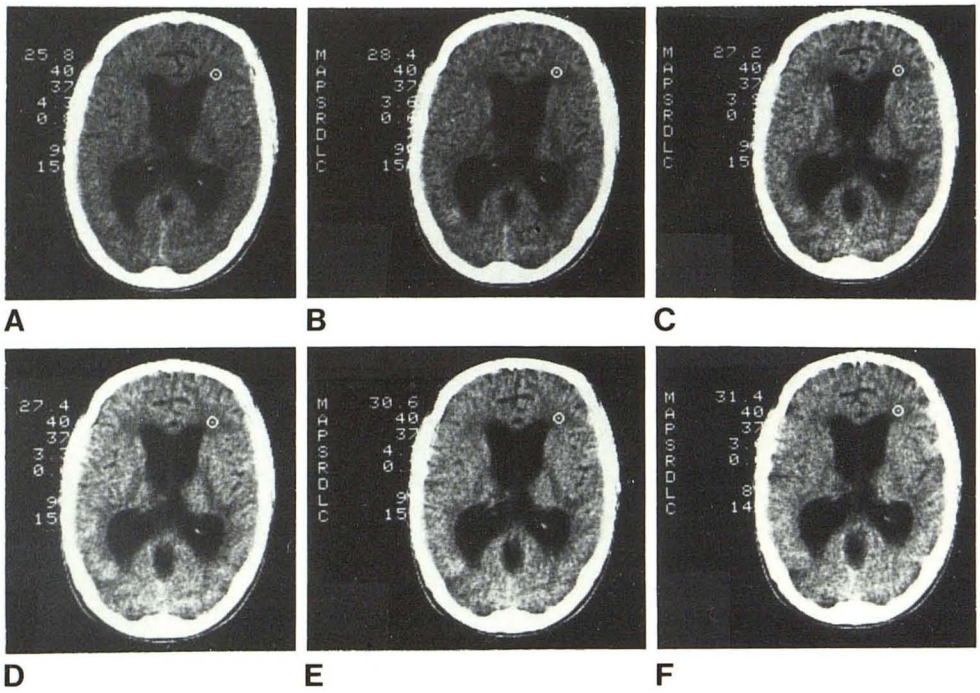

Fig. 11.—Xenon-enhanced CT, buildup analysis of normal periventricular white matter. **A**, Baseline scan before xenon (32%) inhalation with region of interest cursor in periventricular white matter. **B**, 1 min. Mean increase in density (M) somewhat greater than expected for white matter in early stage of inhalation. Good example of difficulties involved in using data from single scan to calculate blood flow, particularly when degree of enhancement is small. **C**, 2.0 min. White matter enhancement less than at 1.0 min, suggesting inaccuracy in 1.0 min scan quantitation due to slight patient movement. **D**, 4.5 min. Enhancement in gray matter continues to exceed that in white matter, and its symmetry is apparent on even visual analysis. **E**, 8.5 min. Increasing enhancement continues in white matter (4.8 CT U, i.e., 30.6–25.8) while gray enhancement is unchanged (equilibrated). **F**, 12.5 min. White matter has not yet approached equilibrium even after 12.5 min of xenon inhalation. If inhalation were continued for 20–30 minutes, xenon concentration in white matter would equilibrate and enhancement would be almost double that in gray matter structures.

flow rate times the arterial concentration ($Q_a = F_a \times C_a$), the venous effluent equals the venous flow rate times the venous concentration ($Q_v = F_v \times C_v$), and the regional tissue concentration (C_i) equals the quantity of tracer (Q_i) taken up by the brain divided by the volume of tissue (V_i): $C_i = Q_i/V_i$. The regional cerebral blood flow (F_i) can then be obtained.

A requirement of a truly regional blood flow method is that the flow rate can be calculated even if venous blood is not available. To do this, the assumption must be made that the inert gas comes into essentially instantaneous diffusion equilibrium between capillary blood and perfused tissue and therefore $C_v = C_i/\lambda_i$. λ_i is the partition coefficient or solubility ratio of the inert gas between a region of brain and blood. By substituting for C_v in the previous equation: $dC_i/dt = (F_i/V_i)(C_a - C_i/\lambda_i)$. Finally, by assuming that the flow in the selected region of brain (e.g., gray matter) is homogeneous, the prior equation may be integrated and solved for C_i (the indicator concentration in a local homogenous region of brain or spinal cord) at any chosen time (T):

$$C_i(T) = \lambda_i K_i \int_0^T C_a(u) e^{-K_i(T-u)} du$$

where K_i is the flow rate constant (per unit weight), C_a the arterial concentration of indicator, and $F_i = \lambda_i K_i$.

The accuracy of this direct tissue saturation technique for calculating rCBF has been extensively validated in laboratory experiments [85–88] and has therefore been applied in many of the in vivo xenon studies [80, 81]. To integrate the arterial concentration $C_a(u)$ over a time interval, multiple sequential arterial blood samples are drawn from the femoral or radial artery and either scanned [79–81] or quantitated in some manner such as fluorescent excitation analysis. A noninvasive method would obviously be superior for clinical purposes and is possible by continuously measuring the end-tidal xenon concentration, if pulmonary function is intact, using a mass spectrometer or xenon thermoconductivity analyzer [82, 83]. The CT clearance profile of inhaled xenon also permits derivation of rCBF in an analogous manner.

Using CT, direct determination of the partition coefficient (λ) in a given tissue compartment (i) can be made by dividing the brain enhancement by the arterial blood enhancement at equilibrium [42, 79–81] with a neglible correction for the specific gravity of brain to obtain flow in the usual units of ml/100 g/min.

$$\lambda_i = \frac{CT\,\#\,Brain\,(at\,equil) - CT\,\#\,Brain\,(baseline)}{CT\,\#\,Blood\,(at\,equil) - CT\,\#\,Blood\,(baseline)}$$

The solubility ratio between brain and blood (λ) determines the distribution of xenon per gram of tissue. Another useful method for calculating λ has been described using Ostwald solubility coefficients [76]. Using this method, it is not necessary to draw arterial blood, since the end tidal xenon concentration at equilibrium may be used:

$$\frac{\Delta CT\,\#}{(Blood)} = \frac{5.15 \times \Theta_{Xe} \times C\,(\%)}{\mu_p^W / \mu_p^{Xe} \times 100}$$

where $\Theta_{Xe} = 0.0011 \times Hct\,(\%) + 0.10$, C = the equilibrium concentration of xenon, and μ_p^W / μ_p^{Xe} is obtained by scanning various concentrations of iodine at specific kilovoltage set-

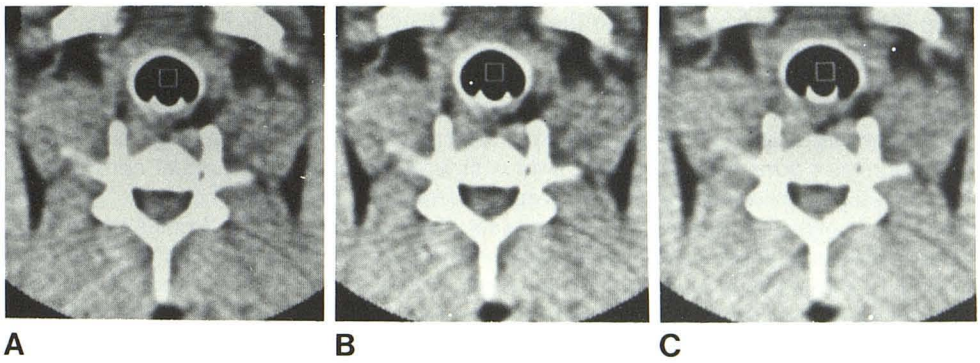

Fig. 12.—Xenon-enhanced CT, buildup analysis of spinal cord. **A**, Baseline nonenhanced CT scan of cervical spinal cord in dog. **B**, 1.5 min. Mild enhancement of cord, but no distinction of gray from white matter (closed system, 50% xenon). **C**, 5.0 min. Greater enhancement of spinal cord with continued xenon inhalation. Derived CT numbers from spinal cord had fairly large deviations making errors fairly large (50% range) when calculating regional spinal cord blood flow and partition coefficient.

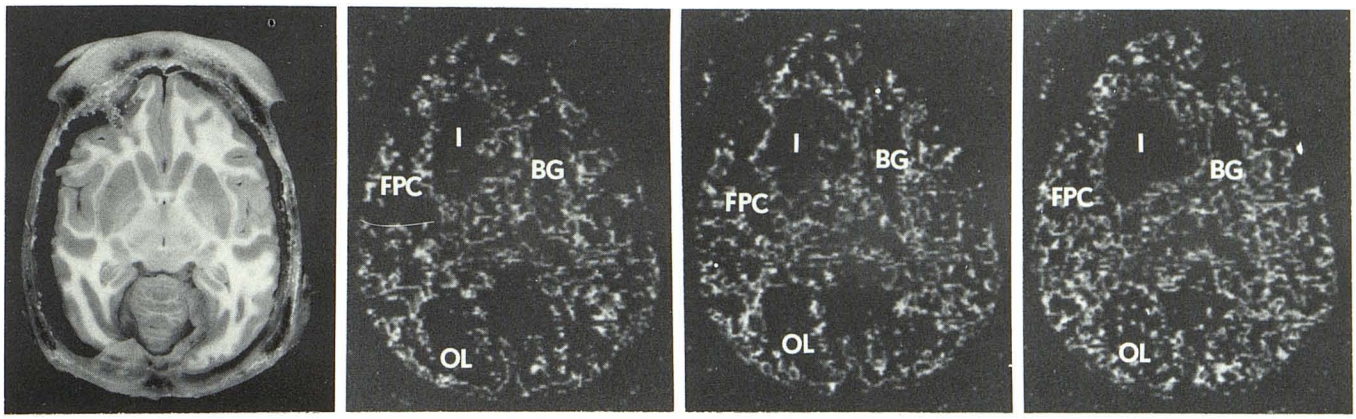

Fig. 13.—Xenon CT, cerebral infarction. **A**, Normal anatomy of baboon at level of sequential xenon study (**B–D**). **B**, 1.5 min Highlighted measure mode display. Decreased enhancement in large area of cerebral infarction (I) produced by surgical cauterization of ipsilateral lenticulostriate branches of the middle cerebral artery. Additional regions of diminished xenon enhancement in homologous contralateral basal ganglia (BG), adjacent opercular cortex (FPC), and ipsilateral occipital lobe (OL). Striking clinical findings included prominent contralateral weakness and homonymous hemianopsia. **C**, 2.5 min. Little change. **D**, 6.5 min. Area of infarction (I) better defined and did not change in density with 14 min of inhalation. Both rCBF and λ are therefore severely decreased in this dead tissue. Contralateral basal ganglia (BG), adjacent opercular cortex (FPC), and occipital lobe (OL) have now enhanced and almost reached equilibrium concentration of xenon confirming normal tissue integrity as reflected by λ but decreased cerebral metabolism as reflected by flow rate constant and rCBF.

tings. This ability to directly calculate the λ of xenon with morphologic specificity is a major advantage of CT compared to the radionuclide method, but there are limitations.

The major uncertainty of the xenon CT technique is biophysical [75, 80, 81]. In essence, the question boils down to what effect on mentation and blood flow a 30%–40% xenon concentration will have, while producing sufficient signal for accurate CT quantitation. Another problem is the difficulty of selecting anatomic regions that sufficiently conform with the basic assumption of homogeneity of flow. To date, all regions of cortical or subcortical gray matter examined in vivo seem to have some, though possibly unimportant, inhomogeneity [80, 89]. Another nontrivial difficulty concerns isolating purely gray from purely white matter with a reasonable CT slice thickness and at the same time accounting for minor patient movement that might occur during the course of the examination. Finally, constant compromises must be made involving radiation exposure, spatial resolution vs. contrast sensitivity, and anatomic precision vs. improved statistical accuracy (e.g., a smaller region of interest gives improved anatomic specificity yet larger error in the derived CT number).

The regional cerebral blood flow and partition coefficient derived from the in vivo "autoradiographic" technique correspond to those determined in vitro. High flow rates with definite regional variation (60–110 ml/100 g/min) have been found in cortical and subcortical gray matter [80–82]. Perfusion rates in white matter have been about 25% those in gray matter (10–25 ml/100 g/min) as expected. Xenon CT measurements have shown anticipated variations in rCBF with changing $Paco_2$ [90]. The directly calculated λ for gray (G) and white (W) matter were also consistent with experimentally derived values (λ_G = 0.8 to 1.0 and λ_W = 1.4 to 1.7). As inhaled xenon will also increase the density of the spinal cord, attempts have been made to calculate spinal cord blood flow and λ [91, 92] (fig. 12). Unfortunately artifact and quantitation difficulties arise when analyzing such a small object surrounded by a bony mass.

To date, most studies with xenon-enhanced CT in either nonhuman primates or man have analyzed cerebral infarc-

tion. The technique has confirmed that both the blood flow and the blood-brain partition coefficient are decreased and heterogeneous within a seemingly homogeneous region of cerebral infarction [81, 83]. The heterogeneity is of therapeutic importance in that the areas with lesser alteration may represent potentially reversible edema or ischemia as opposed to infarction. In addition, a morphysiologic map of flow and λ may be derived for the rest of the cortical, subcortical, and white-matter structures ipsilateral to the infarction and in the contralateral hemisphere. In this manner, areas of the brain that are not directly involved by infarction yet are also hypoperfused may be distinguished (fig. 13). CBF thereby directly reflects brain metabolic activity.

It is important ot recognize that xenon CT studies analyze two distinct yet highly intertwined processes, that is, nutrient blood flow or perfusion of tissue (rCBF) and tissue integrity (λ). Blood flow is derived from the initial, rapidly changing part of the time density buildup or clearance curve, while λ is estimated from the delayed, stable, equilibrium part of the curve (figs. 14 and 15). In xenon CT studies of demyelinating disease (multiple sclerosis), no definite abnormalities were noted [78]. However, the white matter may require 25–30 min to equilibrate. The prolonged inhalation study necessary to precisely analyze tissue integrity in this condition has not yet been performed. Others have affirmed the varying λ in central nervous systems neoplasms [93, 94], but could not differentiate tumor from infarction. Xenon enhancement of the normal cortical mantle may assist in distinguishing an isodense extracerebral hematoma from underlying brain [77]. Studies are also in progress to characterize rCBF and λ in Alzheimer disease, normal aging, and transient ischemic attack. Xenon-enhanced CT has also been used to better define cervical syringohydromyelia [91].

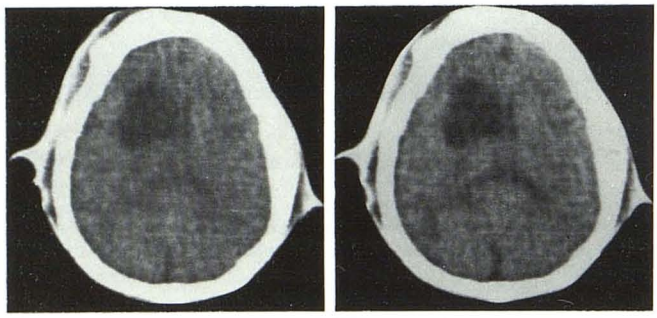

A B

Fig. 14.—Xenon CT, cerebral infarction, primate. **A**, Nonenhanced. **B**, 5 min of xenon inhalation (40%) greatly improves visualization of cerebral infarction, as normal brain enhances and cerebral infarction does not. Xenon may therefore be used to improve morphologic definition on static CT study in addition to its use as blood flow marker.

A minimally invasive, reasonably accurate method for performing xenon CT of selected gray matter at multiple levels with acceptable radiation doses is as follows (figs. 16 and 17). Xenon (35% concentration) is inhaled for 6.5 min and the end-tidal xenon (Ca) is continuously monitored. Obrist et al. [71], in xenon-133 inhalation studies, confirmed that the end-tidal xenon correlates with the arterial xenon concentration if pulmonary function is normal. Using the dynamic scanning mode with rapid table incrementing, three or four levels (4–10 mm collimation) of brain are scanned before enhancement. These same sections are then rescanned during nonradioactive xenon inhalation at 1.5–2 min, 4.0–4.5 min, and 6.0–6.5 min time intervals. The serial scans are then used to measure tissue concentration $C_i(T)$. This scan sequence is the minimum required; more images during the maximum buildup and equilibrium phases would provide more accurate blood flow data. The partition coefficient for gray matter (λ_G) is calculated by dividing the enhancement derived from the 6.0–6.5 min scan of the brain by the concentration of xenon (in CT units) in a venous blood sample. The venous concentration has esentially equilibrated with the arterial concentration by 6.5 min if pulmonary function is intact. If the density (i.e., Δ CT $\neq$) of a given selected gray matter region on the 4.0–4.5 min scans is about equal to that on the 6.0–6.5 min scan, the important theoretical assumption of homogeneity is confirmed. In areas where saturation is not achieved in the inhalation period, curve fitting based on a multivariable analysis can be used to derive both K and λ. At present,

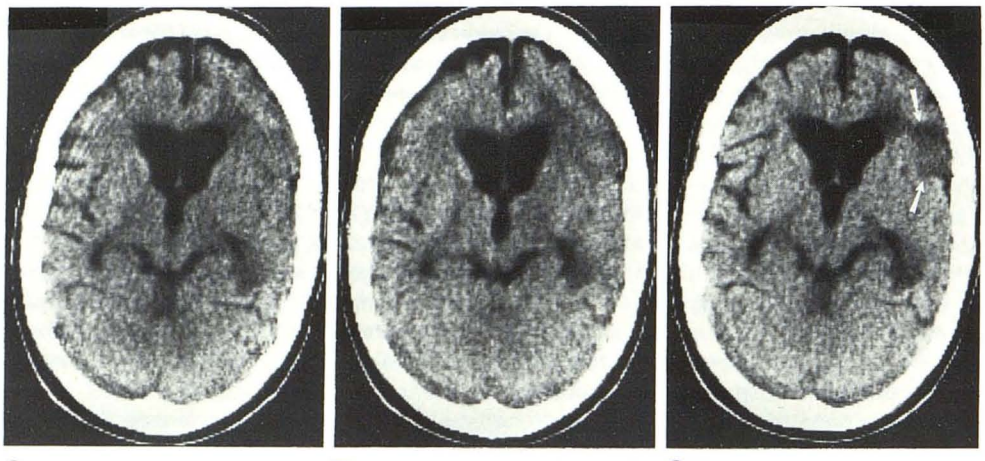

A B C

Fig. 15.—Xenon CT, cerebral infarction, human. **A**, Baseline scan. Area of infarction adjacent to circular sulcus poorly demarcated and might even be missed. **B**, After 2 min of xenon (30%) inhalation. Infarction better seen. **C**, 10 min of inhalation. Previously subtle infarction becomes grossly apparent (*arrows*). rCBF essentially 0 ml/100 g/min in center of infarcted tissue. In ipsilateral caudate nucleus, estimated λ was 0.92 and rCBF was 69.9 ml/100 g/min, both within normal range. Other gray matter locales sampled bilaterally also exhibited normal flow.

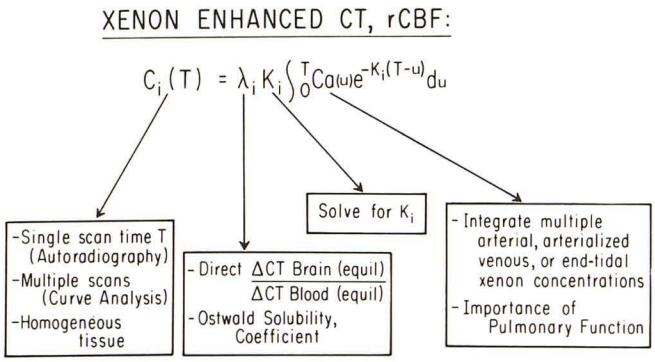

Fig. 16.—Xenon CT, protocol for data acquisition. Basic autoradiographic formula and summary of acquisition of data points.

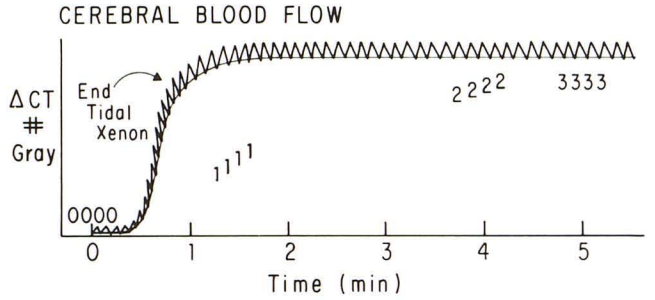

Fig. 17.—Sample of derived data for arterial input function (end tidal xenon represented in CT units) and enhancement from chosen region of gray matter at four different brain levels. 0000 = baseline scans at four levels; 1111 = maximum buildup phase scans at four levels; 2222 = approaching gray matter equilibrium scans at four levels; 3333 = gray matter equilibrium scans at four levels.

relatively simple methods have been used to calculate flow, but more precise methodologies based on more than one image are now being developed [95].

Future Implications

Tissue Characterization and Metabolism

CT will be extremely difficult to surpass as the dominant anatomic imaging method for the central nervous system. Its morphologic specificity permits measurement of various physiologic functions as well. Nevertheless, these successes have highlighted a new challenge, that of investigating brain metabolism with anatomic accuracy. Both emission computed tomography and nuclear magnetic resonance (NMR) carry enormous diagnostic and therapeutic potential for in vivo metabolic imaging.

Can CT compete in this important clinical sphere? Gross tissue analysis is a basic feature of nonenhanced CT scanning as we distinguish gray matter, white matter, cerebrospinal fluid, water, bone, calcium, blood, fat, tumor, and devitalized brain by the percentage of photons they attenuate. Both visual [26] and quantitative [96] attempts have been made to characterize brain edema and distinguish intra- from extracellular brain water. CT scanning may also be used to determine the effective atomic number of a specified structure using dual kilovoltage imaging [27–29]. It has been used with limited success for analyzing the degree of enhancement to differentiate various tumor types [29]. However, its promise for improved in vivo tissue characterization in both health and disease has not been fully developed.

Unique and currently unavailable contrast materials might permit CT to compete as a true metabolic imaging method. Such material should cross the blood-brain barrier (i.e., having high lipid solubility), provide sufficient contrast for CT imaging, remain in the extravascular brain space for a sufficient time at equilibrium concentration after the intravascular component has cleared, define a characteristic metabolic event, and cause no or negligible adverse reactions. These are obviously difficult requirements and call for a redirection of our thoughts about iodinated contrast media and the blood-brain barrier.

The inert gas xenon, with a k-edge and atomic number similar to that of iodine, freely passes the barrier, enhances the brain substance, and selectively localizes in lipid-rich structures (e.g., white matter) at equilibration. Its differential solubility is reflected in the calculation of the brain-blood λ. Unfortunately, none of the other inert gases seem to provide sufficient enhancement for practical CT imaging nor do they appear to selectively define any metabolic function.

There are pharmaceuticals that have been synthesized with radioactive iodine that cross the blood-brain barrier and remain in the brain for a sufficient time to permit equilibrium imaging. These include iodobenzene [97], iodoantipyrine [88, 98], paraiodiamphetamines [99], and iodinated diamines [100], and they may define nonspecific or incompletely characterized metabolic functions. Iodinated radionuclides have also been developed to characterize specific binding to the brain muscarinic cholinergic receptor (iodoquinuclidinylhydroxybenzilate) [101], beta adrenergic receptor, (iodohydroxypindolol) [102], and opiate receptor (iodoenkephalin) [103]. Unfortunately, the toxicity of the large doses of metabolic indicator or ligand required to achieve statistically acceptable x-ray CT enhancement is quite formidable. An example of this type of labeling/toxicity problem was apparent in attempted measurement of rCBF and λ using iodoantipyrine [104]. However, many of these iodinated pharmaceuticals should prove of value using ^{123}I labeling and single-photon-detection emission computed tomography [101, 105, 106] even if the CT approach is unsuccessful. None of the experimental iodinated contrast media that have recently been developed for hepatic and gastrointestinal CT imaging [107–109] seem capable of crossing the blood-brain barrier or delineating specific brain processes. Another approach might involve the use of elements with atomic numbers in the 58–66 range to utilize the effective x-ray energy used in present CT scanners [110].

If a safe and function-specific contrast medium is developed which will not however sufficiently penetrate the blood-brain barrier when infused by the intravascular route, several potential approaches exist to circumvent the barrier. The contrast material may be injected intrathecally as transport *will* normally occur across the CSF-brain barrier [111, 112] (fig. 18). This principle has been repeatedly confirmed in

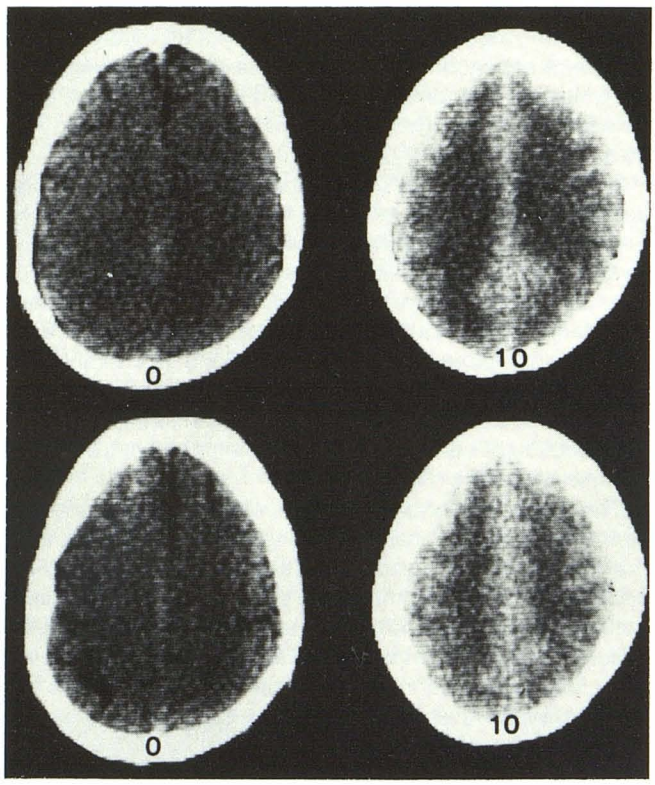

Fig. 18.—Intrathecal metrizamide enhancement, brain "blush." CT scans before (0) and 10 hr after (10) intrathecal introduction by lumbar puncture of metrizamide. At 10 hr, metrizamide readily crosses CSF-brain barrier to enter brain substance. Intrathecal route may be used diagnostically to elucidate abnormality by absence of brain blush or to provide access to brain for large, lipid insoluble indicator. Passage of hydrosoluble, nonionic contrast medium from CSF into brain also accounts for delayed appearance of adverse CNS reactions after myelography.

vivo when delayed scans are performed after intrathecal administration of metrizamide [113, 114]. Unfortunately, many of the adverse reactions related to metrizamide or other iodinated water-soluble contrast media are also likely to be related to this brain penetrance. Another technique for promoting passage of a tissue-specific contrast medium across the barrier involves the use of hypertonic mannitol or arabinose to produce transient opening of the barrier as described above [30–37]. This procedure is experimental; neither its acute nor chronic toxicity has been characterized in large animals or man. Attempts might also be made to manipulate the arterial carbon dioxide levels [115] in order to facilitate transport across the normal or partially damaged barrier.

Advances in Scanner Technology

Although major advances in CT technology may be few in the coming decade, certain modifications could greatly advance the applications of CT for functional imaging. Improvements in contrast sensitivity with reduction in noise would certainly enhance the statistical accuracy of the limited signal often provided by nontoxic doses of contrast materials. CT noise, generally expressed as the standard deviation (SD), has three basic origins: quantum noise, detector efficiency, and mathematical reconstructions. A level of 0.15% noise (i.e., SD of 1.5 on a +1000 to −1000 scale) would assist the interpretation and quantitation of functional images if the sacrifice in spatial resolution were minor.

The easiest means of decreasing the statistical fluctuations of photon flux is to increase the flux (e.g., increase mA, increase scanning time). However, this requires a greater radiation dose and is of particular concern when serial scans are necessary in younger individuals. Higher exposures would also require an x-ray tube with a larger heat capacity if multiple consecutive scans are necessary. On the other hand, the prolonged scanning time would preclude its use for dynamic, nondiffusible indicator, transit time studies. Greater detector efficiency will also decrease noise. The major materials currently used for CT detectors (bismuth germinate, xenon, cadmium tungstate) have limitations of suboptimal efficiency, nonlinearity of response, or afterglow.

Whatever the compromises, scanning flexibility would be enhanced by simple, operator-controlled variation in kilovoltage, amperage, time, and collimation. Further, the ability to readily manipulate the mathematical reconstructions or filter functions should provide the operator the opportunity to select either noise reduction or improved spatial resolution depending on the type of functional study being performed.

Other potentialities for improving the accuracy of quantitative CT imaging are also available. By calculating the effective atomic number of a tissue rather than its derived CT number with dual kilovoltage methods, a truer representation of tissue composition is obtained [27–29]. Moreover, as CT quantitation is dependent on comparing enhanced scans to a previous baseline scan, precise repositioning of regions of interest in the x, y, and z axes is essential. Computerized selection of a specified, density-defined region of interest would assist in selection of a more homogeneous region of interest and in eliminating operator-induced bias.

The scanning of several brain levels simultaneously would provide important additional anatomic coverage during a single functional study. It would be of even greater value to concomitantly scan the carotid artery and thus more readily define the important arterial input function. Accurate methods will need to be developed to superimpose single-photon emission computed tomographic (SPECT) or positron emission tomographic (PET) images on CT images. In this manner, the superb anatomic information provided by CT can be used to better localize the important metabolic and pharmacologic data derived from these radionuclide studies.

Conclusions

Using the unique *anatomic specificity* of x-ray CT, a quantitative map of normal and abnormal brain function can be derived using appropriate contrast media. Th excellent

spatial resolution and rapid scanning time (1–10 sec) are important advantages of x-ray CT over other imaging methods, particularly when analyzing cerebral perfusion. Reasonably accurate in vivo quantitation of blood-brain barrier integrity (delayed iodinated contrast media enhanced CT), regional cerebral blood flow (xenon-enhanced CT), and tissue characterization or lipid content (xenon-enhanced CT, equilibrium stage) in a well defined brain locale is possible using CT imaging.

It would be of major public health and basic scientific importance if the widely distributed CT scanners now available in almost all major health centers in this country could be used to characterize tissue metabolism in addition to their currently established anatomic and physiologic functions. To achieve this, a new class of contrast media will need to be developed. These substances must meet very stringent requirements. They must be of appropriate size and chemical composition to cross the intact blood-brain barrier, yet retain their initial labeled structure. They will need to define a specific biochemical, pharmacologic, or immune characteristic of the central nervous system. Most importantly, these function-specific contrast substances must have minimal toxicity at the doses necessary to provide a sufficient signal for CT quantitation. Due to recent advances in PET scanning technology with improvements in both anatomic specificity and chemical syntheses, it may prove extremely difficult for x-ray CT to compete in this functional sphere. Rapid developments in NMR suggest that these systems may also compete on both a metabolic and a morphologic level.

X-ray CT is a powerful neurodiagnostic tool. Functional applications are natural extensions of this anatomically precise technique. The critical questions are whether in-depth biochemical information can be obtained, and whether this functional information will improve our understanding and treatment of disease or merely provide additional superfluous data. Further experience with currently available methods as well as future developments in contrast media and CT technology will provide the answer to these important questions.

REFERENCES

1. Bertler A, Falck B, Rosengren E. The direct demonstration of a barrier mechanism in the brain capillaries. *Acta Pharmacol Toxicol* **1964**;20:317–321
2. Reese TS, Karnovsky MJ. Fine structural localization of a blood-brain barrier to exogenous peroxidase. *J Cell Biol* **1967**;34:207–217
3. Westergaard E, Brightman MW. Transport of proteins across the normal cerebral arterioles. *J Comp Neurol* **1973**;152:17–44
4. Rapoport SI. *Blood-brain barrier in physiology and medicine*. New York: Raven, **1976**
5. Pardridge WM. Transport of nutrients and hormones through the blood-brain barrier. *Diabetologia* **1981**;20:1–9
6. Bertler A, Falck B, Owman C, et al. The localization of nonaminergic blood-brain barrier mechanisms. *Pharmacol Rev* **1966**;18:369–385
7. Van Gelder NM. A comparison of γ-aminobutyric acid metabolism in rabbit and mouse nervous tissue. *J Neurochem* **1965**;12:239–244
8. Hardebo JE, Owman C. Barrier mechanisms for neurotransmitter monoamines and their precursors at the blood-brain interface. *Ann Neurol* **1980**;8:1–11
9. Drayer BP, Heinz ER, Dujovny M, Wolfson SK, Gur D. Patterns of brain perfusion: dynamic computed tomography using intravenous contrast enhancement. *J Comput Assist Tomogr* **1979**;3:633–640
10. Heinz ER, Dubois PJ, Osborne, D, et al. Dynamic computed tomography study of the brain. *J Comput Assist Tomogr* **1979**;3:641–649
11. Dobben GD, Valvassori GE, Mafee MF, Berninger WH. Evaluation of brain circulation by rapid rotational computed tomography. *Radiology* **1979**;133:105–111
12. Traupe H, Heiss WD, Hoeffken W, Sulch KJ. Perfusion patterns in CT transit studies. *Neuroradiology* **1980**;19:181–191
13. Norman D, Axel L, Berninger WH, et al. Dynamic computed tomography of the brain. Techniques, data analysis, and applications. *AJNR* **1981**;2:1–12
14. Gado MH, Phelps ME, Coleman RE. An extravascular component of contrast enhancement in cranial computed tomography. I. The tissue-blood ratio of contrast enhancement. *Radiology* **1975**;117:589–593
15. Gado MH, Phelps ME, Coleman RE. An extravascular component of contrast enhancement in cranial computed tomography. II. Contrast enhancement and the blood-tissue barrier. *Radiology* **1975**;117:595–597
16. Norman D, Stevens EA, Wing SD, Levin V, Newton TH. Quantitative aspects of contrast enhancement in cranial computed tomography. *Radiology* **1978**;129:683–688
17. Rapoport SI, Levitan H. Neurotoxicity of x-ray contrast media. Relation to lipid solubility and blood brain barrier permeability. *AJR* **1974**;122:186–193
18. Sage MR, Drayer BP, Dubois PJ, Heinz ER, Osborne DO. Increased permeability of the blood-brain barrier after carotid Renografin 76. *AJNR* **1981**;2:272–274
19. Rapoport SI, Hori M, Klatzo I. Testing of a hypothesis for osmotic opening of the blood-brain barrier. *Am J Physiol* **1972**;223:323–331
20. Raporport SI. Opening of the blood-brain barrier by acute hypertension. *Exp Neurol* **1976**;52:467–479
21. Davis JM, Davis KR, Newhouse J, Peister RC. Expanded high iodine dose in computed cranial tomography: a preliminary report. *Radiology* **1979**;131:373–380
22. Hayman LA, Evans RA, Hinck VC. Rapid-high-dose contrast computed tomography of isodense subdural hematoma and cerebral swelling. *Radiology* **1979**;131:381–383
23. Hayman LA, Evans RA, Bastion FO, Hinck VC. Delayed high dose contrast CT. Identifying patients at high risk of massive hemorrhagic infarction. *AJNR* **1981**;2:139–147
24. Older R. Contrast-induced renal failure: a radiological problem and a radiological diagnosis. *Radiology* **1979**;131:553–554
25. Fishman RA. Brain edema. *N Engl J Med* **1975**;293:706–711
26. Drayer BP, Rosenbaum AE. Brain edema defined by cranial computed tomography. *J Comput Assist Tomogr* **1979**;3:317–323
27. Rutherford RA, Pullan BR, Isherwood I. Measurement of effective atomic number and electron density using an EMI scanner. *Neuroradiology* **1976**;11:15–21
28. McDavid WD, Waggener RG, Dennis MJ, Sank UJ, Payne

WH. Estimation of chemical composition and density from computed tomography carried out at a number of energies. *Invest Radiol* **1977**;12:189–194
29. Latchaw RE, Payne JT, Loewenson RB. Predicting brain tumor histology: change of effective atomic number with contrast enhancement. *AJR* **1980**;135:757–762
30. Rapoport SI, Ohno K, Fredericks WR, Pettigrew KD. Regional cerebrovascular permeability to (^{14}C) sucrose after osmotic opening of the blood-brain barrier. *Brain Res* **1978**;150:653–657
31. Brightman MW, Hori M, Rapoport SI, Reese TS, Westergaard E. Osmotic opening of tight junctions in cerebral endothelium. *J Comp Neurol* **1973**;152:317–326
32. Chiueh CC, Sun CL, Kopin IJ, Fredericks WR, Rapoport SI. Entry of (^{3}H) N orepinephune, (^{125}I) albumin and Evans blue from blood into brain following unilateral osmotic osmotic opening of the blood-brain barrier. *Brain Res* **1978**;145:291–301
33. Pappius HM, Savaki HE, Fieschi C, Rapoport SI, Sokoloff L. Osmotic opening of the blood-brain barrier and local cerebral glucose utilization. *Ann Neurol* **1979**;5:211–219
34. Neuwelt EA, Maravilla KR, Frenkel EP, Rapoport SI, Hill SA, Barnett PA. Osmotic blood-brain barrier disruption. *J Clin Invest* **1979**;64:684–688
35. Drayer BP, Schmeckel D, Hedlund L, Lischko M, Sage M, Goulding P. An in vivo CT analysis of transient osmotic opening of the blood-brain barrier. *Radiology* (in press)
36. Neuwelt EA, Frenkel EP, Diehl J, Vu LH, Rapoport SI, Hill S. Reversible osmotic blood brain barrier disruption in man: Implications for the chemotherapy of brain tumors. *Neurosurgery* **1980**;7:44–52
37. Hosegawa H, Allen JC, Mehta BM, Shapiro WR, Posner JB. Enhancement of CNS penetration of methotrexate by hyperosmolar intracarotid mannitol or carcinomatous meningitis. *Neurology* **1979**;29:1280–1286
38. Barranger JA, Rapoport SI, Fredericks WR, et al. Modification of the blood-brain barrier: increased concentration and fate of enzymes entering the brain. *Proc Natl Acad Sci* **1979**;76:481–485
39. Axel L. Cerebral blood flow determination by rapid-sequence computed tomography. *Radiology* **1980**;137:679–686
40. Zierler KL. Equations for measuring blood flow by external monitoring of radioisotopes. *Circ Res* **1965**;16:309–321
41. Oldendorf WH, Kitano M. Radioisotope measurement of brain blood turnover time as a clinical index of brain circulation. *J Nucl Med* **1976**;8:570–587
42. Lassen NA, Ingvar DH. Radioisotope assessment of regional cerebral blood flow. *Progr Nucl Med* **1972**;1:376–409
43. Nylin G, Silverskiold BP, Lofstedt S, Regnstrom O, Hedlund S. Studies on cerebral blood flow in man using radioactive-labelled erthrocytes. *Brain* **1960**;83:293–336
44. Fazio C, Fieschi C, Agnoli A. Direct common carotid injection of radioisotopes for the evaluation of cerebral circulatory disturbances. *Neurology* **1963**;13:561–574
45. Coin CG, Chan YS. Computed tomographic arteriography. *J Comput Assist Tomogr* **1977**;1:165–168
46. Hacker H, Becker H. Time controlled computed tomographic angiography. *J Comput Assist Tomogr* **1977**;1:405–409
47. Meier P, Zierler KL. On the theory of the indicator dilution method for measurement of blood flow and volume. *J Appl Physiol* **1954**;6:731–743
48. Ladurner G, Zilkha E, Iliff LD, DuBoulay GH, Marshall J. Measurement of regional cerebral blood volume by computerized axial tomography. *J Neurol Neurosurg Psychiatry* **1976**;39:152–158
49. Penn RD, Walser R, Kurtz D, Ackerman I. Tumor volume, luxury perfusion and regional blood volume changes in man visualized by subtraction computerized tomography. *J Neurosurg* **1976**;44:449–457
50. Phelps ME, Grubb RL, Ter-Pogossian MM. In vivo regional cerebral blood volume by x-ray fluorescence: validation of method. *J Appl Physiol* **1973**;35:741–747
51. Kuhl DE, Reivich M, Alavi A, Nyary I, Staum MM. Local cerebral blood volume determined by three-dimensional reconstruction of radionuclide scan data. *Circ Res* **1975**;36:610–619
52. Eichling JO, Gado MH, Grubb RL, Larson KB, Raichle ME, Ter-Pogossian MM. Potential pitfalls in the measurement of regional cerebral blood volume. In: Harper M, Jennett B, Miller D, Rowan J, eds. *Blood flow and metabolism in the brain*. Edinburgh: Churchill Livingstone, **1975**:7.15–7.19
53. Phelps ME, Kuhl DE. Pitfalls in the measurement of cerebral blood volume with computed tomography. *Radiology* **1976**;121:375–377
54. Hoedt-Rasmussen K, Skinhoj E, Paulson O, et al. Regional cerebral blood flow in acute apoplexy. The "luxury perfusion syndrome" of brain tissue. *Arch Neurol* **1967**;17:271–281
55. Wolff HG, Forbes HS. The cerebral circulation. IV. The action of hypertonic solutions. *Arch Neurol Psychiatry* **1928**;20:73–83
56. Kagstrom E, Lindgren P, Tornell G. Circulatory disturbances during cerebral angiography. An experimental evaluation of certain contrast media. *Acta Radiol* (Stockh) **1960**;54:3–16
57. Sako Y. Hemodynamic changes during arteriography. *JAMA* **1963**;83:253–256
58. Grubb RL, Hernandez-Perez MJ, Raichle ME, Phelps ME. The effects of iodinated contrast agents on autoregulation of cerebral blood flow. *Stroke* **1974**;5:155–160
59. Dubois PH, Drayer BP, Heinz ER, et al. Rapid sequence cranial computed tomography in tumor evaluation. *Neuroradiology* **1981**;21:79–86
60. Radberg C, Soderlunkh S. Computer tomography in cerebral death. *Acta Radiol [Suppl]* (Stockh) **1975**;346:119–129
61. Drayer BP, Dujovny M, Wolfson SK, et al. Xenon and iodine enhanced CT of diffuse cerebral circulatory arrest. *AJNR* **1980**;1:227–232
62. Heinz ER, Dubois PJ, Drayer BP, et al. Intravenous carotid imaging utilizing the third dimension (abstr). *AJNR* **1980**;1:363
63. Nudelman S, Roehrig H, Seeley G. Intravenous angiography using digital video subtraction. X-ray imaging system. *AJNR* **1980**;1:387–390
64. Nudelman S, Roehrig H. Intravenous angiography using digital video subtraction. Intravenous cervicocerebrovascular angiography. *AJNR* **1980**;1:379–386
65. Strother CM, Sackett JF, Crummy AB, et al. Clinical applications of computerized fluoroscopy. The extracranial carotid arteries. *Radiology* **1980**;136:781–783
66. Meaney TF, Weinstein MA, Buonocore E, et al. Digital subtraction angiography of the human cardiovascular system. *AJR* **1980**;135:1153–1160
67. Kety SS. The theory and applications of the exchange of inert gas at the lungs and tissues. *Pharmacol Rev* **1951**;3:1–41
68. Kety SS. Measurement of local blood flow by the exchange of an inert, diffusible substance. *Methods Med Res* **1960**;8:228–236
69. Lassen NA, Hoedt-Rasmussen K, Sorenson SC, et al. Regional cerebral blood flow in man determined by Krypton-85. *Neurology* **1963**;13:719–727
70. Veall N, Mallett BL. Regional cerebral blood flow determina-

tion by ^{133}Xe inhalation and external recording: the effect of arterial recirculation. *Clin Sci* **1966**;30:353–369
71. Obrist WD, Thompson HK, Wang HS, Wilkinson WE. Regional cerebral blood flow estimated by ^{133}Xenon inhalation. *Stroke* **1975**;6:245–256
72. Kanno I, Lassen NA. Two methods for calculating regional cerebral blood flow from emission computed tomography of inert gas concentrations. *J Comput Assist Tomogr* **1979**;3:71–76
73. Winkler SS, Sackett JF, Holden JE, et al. Xenon inhalation as an adjunct to computerized tomography of the brain: preliminary study. *Invest Radiol* **1977**;12:15–18
74. Haughton VM, Donegan JH, Walsh PR, Syvertsen A, Williams AL. A clinical evaluation of xenon enhancement for computed tomography. *Invest Radiol [Suppl]* **1980**;15:S160–S163
75. Drayer BP, Wolfson SK, Reinmuth OM, Dujovny M, Boehnke M, Cook EE. Xenon enhanced CT for analysis of cerebral integrity, perfusion and blood flow. *Stroke* **1978**;9:123–130
76. Kelcz F, Hilal SK, Hartwell P, Joseph PM. Computed tomographic measurement of xenon brain-blood partition coefficient and implications for regional cerebral blood flow: a preliminary report. *Radiology* **1978**;127:385–392
77. Zilkha E, Kendall BE, Loh L, Hayward R, Radue EW, Ingren S. Diagnosis of subdural hematoma by computed axial tomography: use of xenon for contrast enhancement. *J Neurol Neurosurg Psychiatry* **1978**;41:370–373
78. Radue EW, Kenndall BE. Iodine and xenon enhancement of computed tomography (CT) in multiple sclerosis (MS). *Neuroradiology* **1978**;15:153–158
79. Drayer BP, Gur D, Wolfson SK, Dujovny M. Regional blood flow in the posterior fossa. Xenon enhanced CT scanning. *Acta Neurol Scand [Suppl]* **1979**;60[72]:218–219
80. Drayer BP, Gur D, Wolfson SK, Cook EE. Experimental xenon enhancement with CT imaging: cerebral applications. *AJR* **1980**;134:39–44
81. Drayer BP, Gur D, Yonas H, Wolfson SK, Cook EE. Abnormality of the xenon brain: blood partition coefficient and blood flow in cerebral infarction. *Radiology* **1980**;135:349–354
82. Meyer JS, Hayman LA, Yamomoto M, et al. Local cerebral blood flow measure by CT after stable xenon inhalation. *AJNR* **1980**;1:213–225
83. Meyer JS, Hayman LA, Nakajima S, Yamamoto M, Harati Y. 3-dimensional localized human cerebral blood flow measured in normals and cerebrovascular disorders by CT scanning during stable xenon inhalation (abstr). *Neurology* **1980**;30:445
84. Siesjo BK. Circulation and oxygen consumption in the brain. In: Siesjo BK, ed. *Brain energy metabolism*. Chichester: John Wiley, **1978**:56–100
85. Landau WM, Freygang WH, Rowland LP, Sokoloff L, Kety SS. The local circulation of the living brain: values in the unanesthetized and anesthetized cat. *Trans Am Neurol Assoc* **1955**;80:125–129
86. Freygang WH, Sokoloff L. Quantitative measurement of regional circulation in the central nervous system by the use of radioactive inert gas. *Adv Biol Med Phys* **1958**;6:263–279
87. Eklof B, Lassen NA, Nilsson L, Norberg K, Siesjo BK, Torlof P. Regional cerebral blood flow in the rat measured by the tissue sampling technique: a critical evaluation using four indicators C^{14}-antipyrine, C^{14}-ethanol, H^3-water and xenon^{133} *Acta Physiol Scand* **1974**;91:1–10
88. Sakurada O, Kennedy C, Jehle J, Brown JD, Carbin GL, Sokoloff L. Measurement of local cerebral blood flow with iodo(^{14}C)antipyrine. *Am J Physiol* **1978**;234:H59–H66
89. Reivich M, Slater R, Sano N. Further studies on exponential models of cerebral clearance curves. In: Brock M, Fieschi C, Ingvar DH, Lassen NA, Schurmann K, eds. *Cerebral blood flow. Clinical and experimental results*. New York: Springer, **1969**;8–10
90. Drayer BP, Wolfson SK, Boehnke M, Dujovny M, Rosenbaum AE, Cook EE. Physiologic changes in regional cerebral blood flow defined by xenon-enhanced CT scanning. *Neuroradiology* **1978**;16:220–223
91. Pullicino P, DuBoulay GH, Kendall BE. Xenon enhancement for computed tomography of the spinal cord. *Neuroradiology* **1979**;18:63–66
92. Drayer BP, Hedlund L, Osborne D, Dubois PJ, Heinz ER, Bates M. Spinal cord blood flow using xenon enhanced CT (abstr). *AJNR* **1980**;1:368
93. O'Brien MD, Veall N. Partition coefficients between various brain tumors and blood for ^{133}Xe. *Phys Med Biol* **1974**;19:472–475
94. Radue EW, Kendall BE. Xenon enhancement in tumors and infarcts. *Neuroradiology* **1978**;16:224–227
95. Gur D, Yonas H, Herbert D, et al. Xenon enhanced dynamic CT: multilevel cerebral blood flow studies. *J Comput Assist Tomogr* **1981**;5:334–340
96. Rieth KG, Fujiwara K, Di Chiro G, et al. Serial measurements of CT attenuation and specific gravity in experimental cerebral edema. *Radiology* **1980**;135:343–348
97. Frey K, Boast CA, Wieland D, Brown L, Dudzinski B, Agranoff BW. ^{125}I-iodobenzene as a radiochemical myelin marker (abstr). *Soc Neurosci* **1979**;5:87
98. Uszler LM, Bennett LR, Mena I, Oldendorf WH. Human CNS perfusion scanning with ^{123}I-iodoantipyrine. *Radiology* **1975**;115:197–200
99. Winchell HS, Horst WD, Braun L, Oldendorf WH, Hattner R, Parker H. N-isopropyl (^{123}I) p-iodoamphetamine: single pass brain uptake and washout; binding to brain synaptosomes; and localization in dog and monkey brain. *J Nucl Med* **1980**;21:947–952
100. Kung HF, Blau M. Regional intracellular pH shift: a proposed new mechanism for radiopharmaceutical uptake in brain and other tissues. *J Nucl Med* **1980**;21:147–152
101. Flanagan SD, Storni A. An ^{125}I-labelled binding proven for the muscarinic cholinergic receptor. *Brain Res* **1979**;168:261–274
102. Bylund DB, Charness ME, Snyder SH. Beta adrenergic receptor labeling in intact animals with ^{125}I-hydroxybenzylpindolol. *J Pharmacol Exp Therp* **1977**;201:644–653
103. Chang KJ, Cuatrecasas P. Multiple opiate receptors. Encephalins and morphine bind to receptors with different specificity. *J Biol Chem* **1979**;254:2610–2618
104. Drayer BP, Coleman ER, Bates M, Hedlund L, Petry N. Nonradioactive iodoantipyrine enhanced cranial computed tomography. Preliminary observations. *J Comput Assist Tomogr* **1980**;4:186–190
105. Jaszczak RJ, Chang LT, Stein NA, Moore FE. Whole body single-photon emission computed tomography using dual, large field of view scintillation cameras. *Phys Med Biol* **1979**;24:1123–1143
106. Drayer BP, Jaszczak RJ, Flanagan SD, et al. In vivo analysis of the muscarinic cholinergic receptor using emission computed tomography. Presented at the annual meeting of the American Society of Neuroradiology, Chicago, April **1981**
107. Vermess M, Chatterji DC, Doppmann JL, Grimes G, Adamson RH. Development and experimental evaluation of a contrast medium for computed tomographic examination of the liver and spleen. *J Comput Assist Tomogr* **1979**;3:25–31
108. Violante MR, Dean PB, Fischer HW, Mahoney JA. Particulate

contrast media for computed tomographic scanning of the liver. *Invest Radiol [Suppl]* **1980**;15:5171–5175
109. Young SW, Enzmann DR. Polyvinylpyrrolidone contrast enhancement. Abscess imaging. *Radiology* **1979**;133:511–515
110. Seltzer SE, Paskins-Hurlburt AJ, Hessel SJ. Heavy metal particulate contrast materials for computed tomography of the liver. *J Comput Assist Tomogr* **1980**;4:642–648
111. Davson H. Brain extracellular space and the sink action of cerebrospinal fluid. *Arch Neurol* **1967**;17:196–205
112. Levin I, Sission WB. The penetration of radiolabeled substances into rabbit brain from subarachnoid space. *Brain Res* **1972**;41:145–153
113. Drayer BP, Rosenbaum AE. Studies of the third circulation, Amipaque CT cisternography and ventriculography. *J Neurosurg* **1978**;48:946–956
114. Drayer BP, Rosenbaum AE. Metrizamide brain penetrance. Its correlation with adverse reactions and value radiodiagnostically. *Acta Radiol [Diagn]* (Stockh) **1977**;355:280–293
115. Cutler RW, Barlow CE. The effect of hypercapnea on brain permeability to protein. *Arch Neurol* **1966**;14:54–63